GLOBAL SURFACE AND SUBSURFACE GEOSTROPHIC CURRENTS FROM MULTI-MISSION SATELLITE ALTIMETRY AND HYDROGRAPHIC DATA, 1996-2011

Chi-Hung Chang[1], Chung-Yen Kuo[1], C.K. Shum[2, 3], Yuchan Yi[2], and Ashraf Rateb[1]

Key words: satellite altimetry, GOCE geoid model, surface and sub-surface geostrophic currents, hydrographic profile, NAO, AMOC.

ABSTRACT

Climate indices have been shown to be correlated with changes of absolute ocean current velocities. Yet there has been a lack of available estimates of accurate surface and subsurface current velocities with adequate data span to afford a detailed study. Here, we combined multiple mission satellite altimetry along-track sea surface heights (SSHs), the Gravity field and steady-state Ocean Circulation Explorer (GOCE) time-wise solution generated geoid model, and *in situ* hydrographic data, to estimate global surface and subsurface absolute geostrophic currents, 1996-2011. We used the profile approach to process satellite altimetry data, mitigating the negative impact of omission errors resulting from the spatial resolution discrepancies between the truncated GOCE geoid model and SSHs, on the estimation of the absolute dynamic topography (ADT), which was then combined with the relative dynamic topography derived from *in situ* hydrographic profiles to estimate near global mesoscale geostrophic current velocities at different depth layers. Results were validated by *in situ* moored current meter observations from the Tropical Atmosphere Ocean/TRIangle Trans-Ocean buoy Network (TAO/TRITON) and the Prediction and Research Moored Array in the Atlantic (PIRATA), showing the outperformance of profile approach over the conventional pointwise approach in determination of geostrophic currents. After validating the subsurface geostrophic currents with *in situ* observations from the Kuroshio Extension System Study (KESS) and Line-W projects, statistically significant correlation, between the multi-layer geostrophic current changes for Atlantic Meridional Overturning Circulation (AMOC) branches and the North Atlantic Oscillation (NAO) index, was found, which is in general agreement with other published studies.

I. INTRODUCTION

Ocean circulations play a critical role in transporting sea water, heat, and salinity to the areas they traverse. Bright et al. (2002) indicated that the pathway of the Gulf Stream (GS) is closely associated with the development of the Atlantic tropical cyclones. Ezer et al. (2013) concluded a high correlation between the evolutions of the current velocities of the GS and sea level change along the U.S. mid-Atlantic coast. This strong connection between variations of ocean current velocities and potential natural hazards justifies the desire to monitor the ocean circulations continuously using current meters or Acoustic Doppler Current Profilers (ADCPs), which directly measures surface/subsurface current velocities. In contrast, profiling hydrographic data such as the Array for Real-time Geostrophic Oceanography (Argo) indirectly estimate current velocities from dynamic height derived from temperature and salinity profiling data along Argos floating tracks. As these *in situ* ADCPs have to be deployed via ships and moored in specific locations or sections of the ocean, the difficulties involved in their deployment and maintenance result in *in situ* current velocity measurements at small-scale or only with regional coverage. The joint use of satellite altimetry and hydrographic profiling data has a distinct advantage for its feasibility to measure long-term global surface and subsurface geostrophic current velocities, which is the rationale of our study.

Wunsch and Gaposchkin (1980) proposed a pioneering theory to determine absolute surface geostrophic currents on the basis of absolute dynamic topography (ADT) derived by using a geoid model as the referenced datum of sea surface heights (SSHs), instead of using the relative surface geostrophic currents and based on assuming a "level of no-motion" in the deep

ocean. The "level of no-motion" assumption, which is invalid over the global ocean, was once widely applied in conventional oceanography. Subsurface geostrophic currents can also be obtained when ADT is further combined with relative dynamic topography (RDT). The idea was not feasible at the time when Wunsch and Gaposchkin published their paper because of the lack of highly accurate SSHs and an accurate Earth's gravity field with adequate resolution until the 1990s. Since 1992, the advent of TOPEX/POSEIDON (T/P) satellite altimetry is the dawn of the age of satellite-borne long-term global synoptic SSH measurements with unprecedented resolution, sampling and accuracy. The advent of satellite gravimetry missions launched a decade later drastically improved global gravity field or geoid modeling to enable more accurate estimates of absolute surface geostrophic currents. The CHAllenging Minisatellite Payload (CHAMP) and the Gravity Recovery and Climate Experiment (GRACE) gravimetry mission data have provided significant improvement in the global geoid models longer than spherical harmonic degree 150, and enabled steady improvement of global surface geostrophic current estimates. Since 2009, the Gravity field and steady-state Ocean Circulation Explorer (GOCE) satellite has advanced global geoid models to an accuracy of 1-2 cm at spatial resolution better than 100 km (European Space Agency, 1999). The GOCE derived geoid models have been shown to outperform GRACE geoid models in the determination of absolute surface geostrophic currents (Sánchez-Reales et al., 2012; Feng et al., 2013).

Given that pure satellite-gravimetry-observed gravity field models (hereafter referred to as satellite-only gravity field model) only provide a truncated spectrum, taking a geoid model determined from a satellite-only gravity field model (hereafter referred to as a satellite-only geoid model) as datum of SSHs to define ADT results in the retention of most of the omission errors caused by spatial resolution discrepancies. These errors, which differ from the commission errors caused by the gravity field observation itself, can severely contaminate the ADT, and the resulting estimated geostrophic current velocities (Bingham et al., 2008). The most straightforward processing strategy to mitigate the impact of these errors and ensure the resolution of SSHs and the satellite-only geoid model are compatible is the use of the "pointwise approach." In this approach, a 2-dimensional (2D) spatial filter is applied to both the SSHs and the satellite-only geoid model. However, this approach does not involve preprocessing to deal with the contamination of geoid omission errors. A wider filter radius is needed to effectively ease the problem, which also leads to the unwanted additional attenuation of oceanic signals. The pointwise approach is also made ineffective by the fact that a 2D spatial filter can only assimilate limited data near the ocean-land boundary into the filter kernel (which is negatively affected by omission errors), primarily because of the lack of altimetric observations on land (Bingham et al., 2008), and also because altimetric observations are less accurate in the coastal regions due to land contamination, more media and geophysical correction errors, such as tides. Another approach is the spectral approach (Bingham et al., 2008), which

has been widely applied to process Mean Dynamic Topography (MDT); however, its core principle is to form a hybrid mean sea surface (hybrid-MSS) that can generate a pattern of omission errors similar to that of the satellite-only geoid model through truncation. The omission errors can then be mitigated during the subtraction. The spectral approach requires high-resolution grids with small-scale features near ocean-land boundaries and islands to effectively mitigate the altimeter data outage problem. The same was achieved by Bingham et al. (2008) who used MSS-CLS01 mean sea surface model with a two arc minute resolution. However, adopting the spectral approach to process time-variant, along-track data with a comparatively sparse distribution results in a gridded ADT, which mostly results from interpolation or extrapolation. Thus, the quality of ADT highly depends on the interpolation or extrapolation algorithm applied to form a high-resolution grid, which can be quite inaccurate near coastal regions.

The present study adopts the profile approach (Bosch and Savcenko, 2010) to process along-track SSHs and the GOCE geoid model to generate ADT. The ADT is then combined with the RDT to determine geostrophic currents at surface and subsurface depth layers (Wunsch and Gaposchkin, 1980; Cadden et al., 2009). Furthermore, recent studies all employed the GOCE geoid model as the MDT datum to determine mean surface geostrophic currents (Sánchez-Reales et al., 2012; Feng et al., 2013). In this way, our study further extends to the estimation of global subsurface geostrophic current velocities, and using long-term multiple satellite altimetry and hydrography data, 1996-2011, to enable study of time variant current velocities globally. Prior to this study, the performance or validation of geostrophic currents at the subsurface layers, has yet been quantified (e.g., Cadden et al., 2009). Here we compare our satellite-derived results with *in situ* and ground truth current meter observations from numerous moored stations. Finally, we use the estimated long-term surface and subsurface current speed in the branches of the Atlantic Meridional Overturning Circulation (AMOC), to study their correlation with the North Atlantic Oscillation (NAO) index (Hurrell, 1995).

II. DATA

1. Satellite Altimetry

Along-track 1 Hz altimetry SSHs referenced to the TOPEX ellipsoid observed by T/P, ERS-2, Envisat, and Jason-1/-2 satellites from 1996 to 2011 are processed using the Radar Altimeter Database System (RADS) (Scharroo et al., 2013). Instrumental, media (i.e., ionospheric, dry and wet tropospheric corrections), and geophysical (i.e., orbit, solid tide, ocean tide, tidal loading, pole tide, atmosphere barotropic response, and sea state bias) corrections are applied to the SSHs. Since the negative impacts in the ADT and resulting geostrophic currents are due to the omission errors caused by spatial resolution discrepancies between altimetry SSHs and satellite-only geoid model, the enhancement of results by using 18-20 Hz along-track altimetry SSHs is quite limited. Moreover, the higher

Table 1. Temporal coverage of satellite altimetry data used in the study.

Satellite	Temporal Coverage
ERS-2	1996/01-2002/12
Envisat	2003/01-2011/12
T/P	1996/01-2002/07
Jason-1	2002/08-2008/12
Jason-2	2009/01-2011/12

frequency altimetry SSHs are noisier, so smoothing process is required to mitigate the noises within. Besides, even though the 18-20 Hz along-track altimetry SSHs can be observed closer toward land, the observations contain more errors. Therefore, the full resolution altimetry SSHs give no significant advance than 1 Hz along-track data.

The 1 Hz SSHs observed by different satellites are then merged to generate multi-satellite SSHs by applying relative biases estimated by RADS relative to T/P. T/P and Jason-1 shifted their nominal repeat orbital tracks to interleave orbits, during August and September 2002, and in February 2009, respectively. Therefore, altimetric observations after these orbital track shifts are excluded in this study to ensure that the SSHs from T/P, Jason-1, and Jason-2 have the same ground tracks. However, the use of the observations during the shift of the Envisat track in October 2010 is desirable to stretch the temporal coverage to the end of 2011. With such a data selection scenario, all the monthly along-track SSHs in this study is a combination of observations from two distinct or different repeat orbits, 10-day and 35-day repeat orbits (Table 1).

2. Geoid Model

The study uses the 4th generation GOCE time-wise gravity field model (GOCE-TIM4) (Pail et al., 2011), to determine the geoid model using Bruns' formula (Heiskanen and Moritz, 1967). The maximum spherical harmonic expansion degree (L) of the GOCE-TIM4 is up to 250. The model is derived from pure GOCE gravity gradient observations from November 1, 2009 to June 19, 2012 with no external gravity information either as a reference model or to constrain the solution during the gravity field inversion process. The Earth Gravitational Model 2008 (EGM2008) (Pavlis et al., 2012) is an ultra-high resolution gravity field model with L up to 2,190 that was developed by a least squares procedure and combined with the ITG-GRACE03S gravity field model, which has an L up to 180 with 57 months' GRACE observations, including its associated error covariance matrix (Mayer-Gürr, 2007), and the global set of five arc minute area-mean free-air gravity anomalies. These anomalies are determined by the integration of satellite altimetry, air-borne, marine, and terrestrial gravity data. EGM2008 with ultra-high spatial resolution is taken as a proxy of the SSHs required in the profile approach. Both gravity field models can be downloaded under the service of the International Center for Global Earth Models (ICGEM). EGM2008 should not be

taken as datum of SSHs because it already contains altimetric data during the generating process and doing so could lead to the elimination of altimetric signals when being subtracted from SSHs (Janjić et al., 2012). Both geoid models should be based on the TOPEX ellipsoid as SSHs.

3. Hydrographic Data

Ishii and Kimoto (2009) published a set of $1° \times 1°$ global gridded monthly hydrographic profiles (temperature/salinity) by integrating the temperature data from the World Ocean Database (WOD05), and the salinity data from the World Ocean Atlas (WOA05). Since 1990, the near real-time data from the Global Temperature and Salinity Profile Program (GTSPP) has been used to compensate for the sparseness of the WOD05 data. Moreover, observations from expendable bathythermograph (XBT) compiled by the Japan Oceanographic Data Center (JODC) have also been adopted. The latest version 6.13 extends the temporal coverage from 1945 to 2012 with 24 Levitus depth layers from 0 m to 1,500 m. This version integrates the latest WOD09, GTSPP, and Argo data provided by Global Data Assembly Centers (GDAC). Depth bias corrections in WOA05 and XBT have also been updated. The data are released from the Research Data Archive (RDA) managed by the Data Support Section of the Computational and Information Systems Laboratory (CISL) at the National Center for Atmospheric Research (NCAR). In the study, the hydrographic profile data span used encompasses that for the along-track altimetric SSHs from 1996 to 2011.

4. Maps of Absolute Geostrophic Currents

The $0.25° \times 0.25°$ gridded maps of absolute geostrophic currents based on the all-satellite merged ADT, processed and distributed by the Archiving, Validation and Interpretation of Satellite Oceanographic data (AVISO), are used to compare with our resulting geostrophic currents at the sea surface. The all-satellite merged ADT combines SSHs from whole missions available, up to 4 satellites among HaiYang-2A (HY-2A), Saral/AltiKa, Cryosat-2, Jason-1, Jason-2, T/P, Envisat, Geosat-Follow-On (GFO) and ERS-1/-2 at a given time and is with respect to the geoid model generated from the 4th generation GOCE direct solution gravity field model (GOCE-DIR4). GOCE-DIR4 contains 7-year GRACE and 2-year reprocessed GOCE data (Bruinsma et al., 2013). The dataset also assimilates the Coriolis Ocean database ReAnalysis (CORA) 3.4 hydrogra-phic database (Cabanes et al., 2013), containing *in situ* hydrographic observations for the computation of the ocean dynamic heights and the drifting buoy velocities distributed by the Surface Drifter Data Assembly Center (SD-DAC), covering the period 1993-2012 (Hansen and Poulain, 1996), to compensate the small scale (< 100 km) features (Rio et al., 2013).

## 5. *In situ* Current Velocities

The monthly averages of the *in situ* current velocities recorded by 28 moored stations fixed at 10 m depths are obtained from the Tropical Atmosphere Ocean/TRIangle Trans-Ocean buoy Network (TAO/TRITON) (McPhaden et al., 1998) and

Table 2. Locations of 28 moored stations (Sta.) of TAO/TRITON and PIRATA.

	TAO/TRITON						PIRATA	
Sta.	Location	Sta.	Location	Sta.	Location	Sta.	Location
1	8°N, 137°E	8	5°N, 235°E	15	2°S, 220°E	22	20°N, 332°E
2	8°N, 156°E	9	5°N, 265°E	16	2°S, 235°E	23	21°N, 337°E
3	9°N, 220°E	10	2°N, 137°E	17	2°S, 265°E	24	15°N, 332°E
4	8°N, 265°E	11	2°N, 147°E	18	5°S, 235°E	25	12°N, 337°E
5	5°N, 137°E	12	2°N, 156°E	19	5°S, 265°E	26	3.5°N, 337°E
6	5°N, 147°E	13	3.5°N, 265°E	20	8°S, 235°E	27	6°S, 8°E
7	5°N, 156°E	14	2°S, 156°E	21	8°S, 265°E	28	10°S, 350°E

Table 3. Locations of KESS moored stations.

| Station	Depth (m)	2004/07-2005/05	2005/07-2006/04
2	1,500	36.31°N, 146.89°E	36.36°N, 146.85°E
3	1,500	35.55°N, 146.43°E	35.55°N, 146.41°E
4	250 and 1,500	34.18°N, 146.21°E	34.85°N, 146.02°E
5	250 and 1,500	34.03°N, 145.52°E	34.03°N, 145.51°E
6	1,500	33.24°N, 145.03°E	33.29°N, 145.04°E
7	1,500	32.40°N, 144.55°E	32.41°N, 144.59°E
8	1,500	N/A	34.83°N, 145.00°E
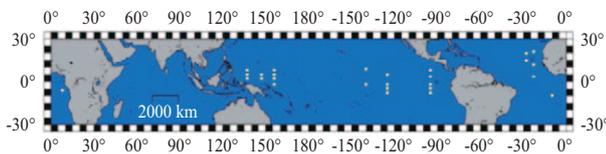
Fig. 1. Distribution of 28 moored stations of TAO/TRITON and PIRATA.

Prediction and Research Moored Array in the Atlantic (PIRATA) (Bourles et al., 2008) projects (Fig. 1 and Table 2), at the National Oceanic and Atmospheric Administration/Pacific Marine Environmental Laboratory (NOAA/PMEL). The projects provide *in situ* observations from the most number of stations and homogenous coverage over low and mid-latitude regions fixed at the same depth. Thus, the projects are consistently used to conduct performance analysis and validation near the sea surface.

The *in situ* observations from the Kuroshio Extension System Study (KESS) (Jayne et al., 2009; Waterman et al., 2011) and the Line-W (http://www.whoi.edu/science/PO/linew) projects at the Woods Hole Oceanographic Institution (WHOI), are used to validate our results at the subsurface layers.

The field experiment of KESS was conducted from the summer of 2004 to the summer of 2006. KESS aims to understand the processes coupling the baroclinic and barotropic circulation and variability. It also aims to determine and quantify the cross-frontal exchange processes in the Kuroshio Extension (KE) and the processes governing the strength and structure of the position, elongation, stratification and subtropical mode of the water
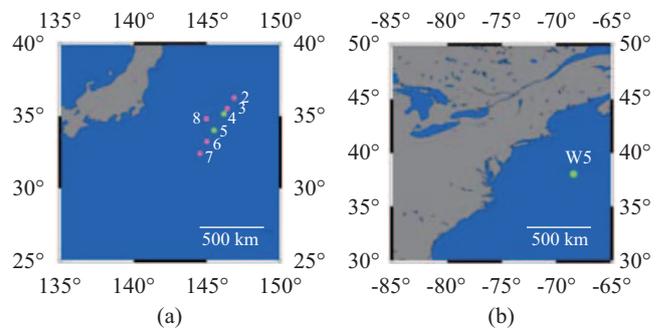
Fig. 2. Locations of (a) KESS and (b) Line-W's W5 stations. Their data are used to validate the satellite altimetry estimated geostrophic currents at the subsurface layers. The green dots mark the stations with multi-depth observations, while the red dots are the stations with observations fixed at the same depth.

formation within the recirculation gyre. Current velocities are observed at fixed depths of 250 and 1,500 m (Fig. 2(a) and Table 3) using a vector averaging current meter (VACM). Station 1 has no available VACM observations. Line-W is a long-term climate observing system which is focused on monitoring the deep limb of the AMOC and has been fully operating in the North Atlantic Ocean since 2003. Line-W observations will contribute to the enhancement of our understanding about the response of ocean circulation to the North Atlantic air-sea exchange. Current velocities are observed with an acoustic current meter. The Station W5 data that comprise profile observations under a depth

Table 4. Location of Line-W's W5 moored stations. The current meter profile is under the depth of 1,000 m. The depths corresponding to hydrographic data (Ishii and Kimoto, 2009) are selected (1,100, 1,200, 1,300, 1,400, and 1,500 m).

Time	Location
2004/06-2005/03	38.04°N, 291.60°E
2005/05-2006/03	38.09°N, 291.62°E
2006/05-2007/03	38.11°N, 291.66°E
2007/04-2008/04	38.04°N, 291.60°E

of 1,000 m from 2004 to 2008 are adopted as ground truth. The five depths selected in this study correspond to the depth layers of the hydrographic profile (Ishii and Kimoto, 2009) (Fig. 2(b) and Table 4).

The non-geostrophic currents, including Ekman and wave-induced currents, for all the *in situ* current velocity observations are determined with the algorithm proposed by Weber (1983) (see also Ohashi et al., 2013), and by using the sea surface wind velocities provided by the National Climatic Data Center (NCDC) (Zhang et al., 2006a; 2006b). The temporal coverage of *in situ* observations used in the study follows the sea surface wind velocities with complete 12-month data from 1996 to 2010.

6. North Atlantic Oscillation

In measuring the NAO throughout the year, several indices are used to track the seasonal movements of the Icelandic low and Azores high. One of the indices is the principle-component-based NAO (PC-based NAO) index (Hurrell, 1995), which is the time series of the leading empirical orthogonal function of sea level pressure anomalies over the Atlantic section (20°-80°N, 90°W-40°E). The PC-based NAO index can be obtained from the Climate Data Guide (CDG) of the National Center for Atmospheric Research/University Corporation for Atmospheric Research (NCAR/UCAR). The positive phase of the NAO is typically associated with stronger-than-average westerlies over the mid-latitudes, considerably intense weather over the North Atlantic, and mild weather over Western Europe. The PC-based NAO index is a more optimal representation of the full spatial patterns of the NAO and is less noisy than station-based data sets. The temporal span of the NAO covers 1996-2011.

III. METHODOLOGY

1. Processing Absolute Dynamic Topography

The processing procedure of the conventional pointwise approach is straightforward, that is, it simply adopts a 2D spatial Gaussian filter (also for gridding) (Chambers et al., 1997) for the ADT generated by subtracting the satellite-only geoid model from along-track SSHs. The equation is as follows:

$$\eta_{abs} = \left[h - N_{Sat.} \right]^{\dot{f}_{2D}} \tag{1}$$

where η_{abs} is the ADT; h and N_{Sat} are the along-track SSHs and satellite-only geoid model, respectively. η_{abs} is then smoothed

by the 2D spatial Gaussian filter ($\dot{f}_{2D}$). Given that the spatial resolution of the GOCE-TIM4 is 0.72° based on the 180°/L relation, where L is 250, the basic filter radius (half-width at half-maximum of Gaussian function) applied in this study is 0.72°, then gradually expands to 1.00° and 1.13°.

The profile approach (Bosch and Savcenko, 2010), which is aimed at processing time-variant, along-track data, is applied to mitigate the errors retained in the ADT. The main motivation of the profile approach is to avoid the initial gridding of the SSHs in order to preserve more along-track high resolution altimetry data. Also, the artificial extension of SSHs toward land which is mostly filled with geoid model shall be bypassed with the risk to generate Gibbs effect in ocean-land transition zone (Bosch et al., 2012). To do so, the objective is to filter the along-track SSHs as the satellite-only geoid model but only at where they are observed. The process can be expressed concisely as follows:

$$\eta_{abs} = (h^{\dot{f}_{1D}} - N_{EGM\,2008}^{\dot{f}_{1D}}) + (N_{EGM\,2008}^{\dot{F}_{2D}} - N_{Sat.}^{\dot{F}_{2D}}) \tag{2}$$

where $h^{\dot{f}_{1D}}$ and $N_{EGM\,2008}^{\dot{f}_{1D}}$ are the along-track SSHs and EGM2008 geoid model, respectively, both of which are smoothed by a 1D along-track Gaussian filter in the spatial domain ($\dot{f}_{1D}$). $N_{EGM\,2008}^{\dot{F}_{2D}}$ and $N_{Sat.}^{\dot{F}_{2D}}$ are the EGM2008 geoid model and satellite-only geoid model, respectively. Both models are smoothed by a 2D spectral Gaussian filter ($\dot{F}_{2D}$) (Jekeli, 1981) in the form of the spectral gravity field model and subsequently converted to the spatial domain by Bruns' formula (Heiskanen and Moritz, 1967) along the tracks.

The filter radius (half-width at half-maximum of Gaussian function) of the profile approach is based on the empirical formula proposed by Zenner (2006):

$$\frac{14500(km)}{L} \cong \frac{130^{o}}{L} \tag{3}$$

A Gaussian distance-weighted function is applied after the profile approach process to generate a gridded ADT with the same filter radius as that in the pointwise approach.

2. Geostrophic Currents

Geostrophic currents at each depth layer based on *f*-plane geostrophic approximation can be calculated using the following
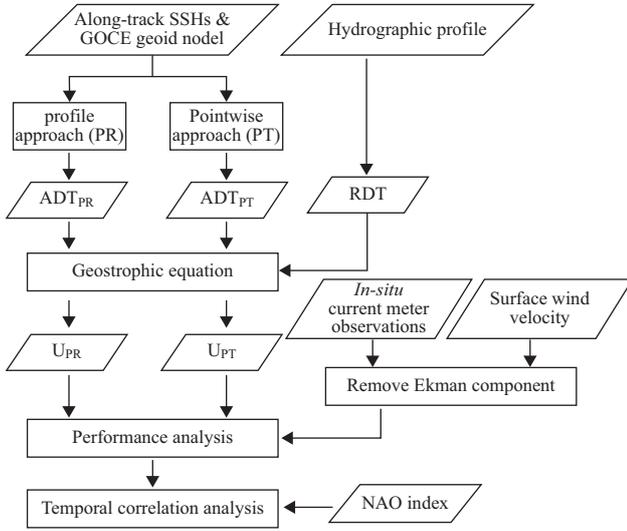
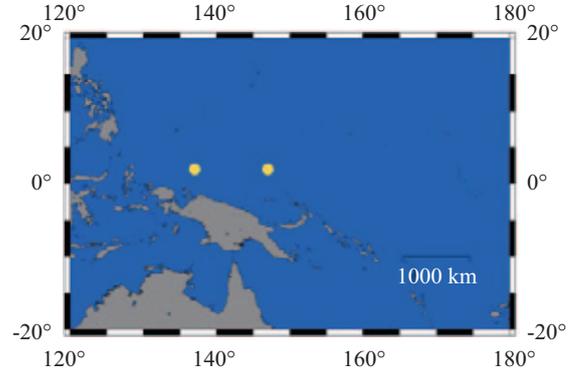**Fig. 3. Flowchart of research progress.**

Fig. 4.   Stations where pointwise approach gives RMS that were larger than the average RMS by three-time STD. The stations are near New Guinea in the western Equatorial Pacific.

equation (Wunsch and Gaposchkin, 1980):

$$U_R = u_R + v_R i$$
$$= \frac{g}{f}\left(-\frac{\partial \eta_{res}}{\partial y} + \frac{\partial \eta_{res}}{\partial x} i\right) \quad (4)$$

where U_R is the geostrophic current velocities at each depth layer, with u_R and v_R denoting zonal and meridional directions, respectively. An imaginary unit ($i = \sqrt{-1}$) is used to express zonal and meridional components with real and imaginary numbers, respectively. x and y are the zonal and meridional distances, which are positive in the eastward and northward directions, respectively. g is the gravitational acceleration, and $f = 2\Omega \cdot \sin\varphi$ is the Coriolis parameter with the mean Earth rotation rate Ω and latitude φ. The term η_{res} in Eq. (4) can be computed as follows:

$$\eta_{res} = \eta_{abs} - \eta_{rel} \quad (5)$$

where η_{rel} is the RDT, which can be calculated by integration (Cadden et al., 2009)

$$\eta_{rel} = 0.1 \times \int_{P_R}^{0} \frac{dp}{\rho} \quad (6)$$

where P_R is the specific pressure level, p is the pressure, and ρ is the sea water density derived on the basis of the international equation of state of seawater 1980 (IES 80) (Millero and Poisson, 1981). Given that the integration of the inverse of ρ with p only provides geopotential distance, it should be further multiplied by "0.1" to approximate the "dynamic meter," which is geometrically equal to the "meter" of the physical displacement in the vertical direction.

The β-plane geostrophic approximation, which has been proved to be in good agreement with the observed velocities in the Equatorial Undercurrent (Lukas and Firing, 1984; Picaut et al., 1989), was applied because f approaches zero near the equator, thus offering an unstable solution. The weighted combination of the results from the f-plane and β-plane geostrophic approximation forms a smooth connection between the results within and outside the equatorial band (5°S-5°N) (Lagerloef et al., 1999).

IV. RESULTS AND DISCUSSION

According to the research progress as shown in Fig. 3, the results are computed and analyzed as follows.

1. Performance Analysis on Profile Approach

The performance of the profile approach and pointwise approach in determining geostrophic current velocities was compared with the available *in situ* current velocities from the TAO/ TRITON and PIRATA projects, as ground truth, after the non-geostrophic components removed. The stations whose root mean square (RMS) given by the pointwise approach was larger than the average RMS by three-time standard deviation (STD) were analyzed. These stations included stations 10 and 11. Fig. 4 illustrates that these stations with poor accuracy are distributed near the islands or near lands (areas that are most negatively affected by omission errors). This result proves the limitation of the pointwise approach near the ocean-land boundary.

Table 5 shows the comparison between the performance of the profile approach and pointwise approach at Stations 10 and 11. A significant improvement can be observed in the adoption of the profile approach. The profile approach achieved the highest rate of improvement (ROI) of up to 83% at Station 11 in the meridional direction. The ROI can also reach up to 24-60% for the other components. Hence, using the ADT processed with the profile approach to determine geostrophic current velocities can attain excellent accuracy at stations near the ocean-land boundary.

Station 11, where the RMS given by the profile approach was higher than the average RMS by three-time STD, was further

Table 5. Comparison of RMS (cm/s) and ROI at Stations 10 and 11 given by the profile approach (PR) and pointwise approach (PT) under different gridding filter radii.

Filter radius	Station 10		
	RMS (PT) (cm/s) $\begin{pmatrix} u_R \\ v_R \end{pmatrix}$	RMS (PR) (cm/s) $\begin{pmatrix} u_R \\ v_R \end{pmatrix}$	ROI (%) $\begin{pmatrix} u_R \\ v_R \end{pmatrix}$
0.72°	$\begin{pmatrix} 54.0 \\ 31.0 \end{pmatrix}$	$\begin{pmatrix} 39.9 \\ 13.7 \end{pmatrix}$	$\begin{pmatrix} 26 \\ 56 \end{pmatrix}$
1.00°	$\begin{pmatrix} 54.8 \\ 21.0 \end{pmatrix}$	$\begin{pmatrix} 39.8 \\ 12.6 \end{pmatrix}$	$\begin{pmatrix} 27 \\ 40 \end{pmatrix}$
1.13°	$\begin{pmatrix} 54.3 \\ 17.8 \end{pmatrix}$	$\begin{pmatrix} 39.7 \\ 12.2 \end{pmatrix}$	$\begin{pmatrix} 27 \\ 32 \end{pmatrix}$
	Station 11		
0.72°	$\begin{pmatrix} 42.1 \\ 151.7 \end{pmatrix}$	$\begin{pmatrix} 16.6 \\ 25.6 \end{pmatrix}$	$\begin{pmatrix} 60 \\ 83 \end{pmatrix}$
1.00°	$\begin{pmatrix} 29.1 \\ 110.0 \end{pmatrix}$	$\begin{pmatrix} 17.4 \\ 19.8 \end{pmatrix}$	$\begin{pmatrix} 40 \\ 82 \end{pmatrix}$
1.13°	$\begin{pmatrix} 23.8 \\ 91.4 \end{pmatrix}$	$\begin{pmatrix} 18.1 \\ 17.4 \end{pmatrix}$	$\begin{pmatrix} 24 \\ 81 \end{pmatrix}$

Table 6. Comparison of average RMS with STD of over 27 stations given by the profile approach (PR) and pointwise approach (PT), percentage (Per.) of stations where the profile approach results in a smaller RMS than the pointwise approach, and the ROI of the profile approach under different gridding filter radii. The average ratio of the resulting RMS over the absolute maximum in situ current velocities is also shown.

Filterradius	Average RMS ± STD (cm/s) and ratio (%) $\begin{pmatrix} u_R \\ v_R \end{pmatrix}$		Per. (%) $\begin{pmatrix} u_R \\ v_R \end{pmatrix}$	ROI (%) $\begin{pmatrix} u_R \\ v_R \end{pmatrix}$
	PT	PR		
0.72°	$\begin{pmatrix} 15.5 \pm 13.4 \\ 16.3 \pm 11.1 \end{pmatrix}$ $\begin{pmatrix} 43 \\ 76 \end{pmatrix}$	$\begin{pmatrix} 11.2 \pm 7.7 \\ 8.8 \pm 3.5 \end{pmatrix}$ $\begin{pmatrix} 32 \\ 44 \end{pmatrix}$	$\begin{pmatrix} 78 \\ 81 \end{pmatrix}$	$\begin{pmatrix} 15 \\ 32 \end{pmatrix}$
1.00°	$\begin{pmatrix} 14.7 \pm 12.4 \\ 13.0 \pm 7.6 \end{pmatrix}$ $\begin{pmatrix} 40 \\ 60 \end{pmatrix}$	$\begin{pmatrix} 11.5 \pm 7.6 \\ 8.5 \pm 3.2 \end{pmatrix}$ $\begin{pmatrix} 33 \\ 42 \end{pmatrix}$	$\begin{pmatrix} 67 \\ 78 \end{pmatrix}$	$\begin{pmatrix} 10 \\ 23 \end{pmatrix}$
1.13°	$\begin{pmatrix} 14.5 \pm 12.0 \\ 12.0 \pm 6.6 \end{pmatrix}$ $\begin{pmatrix} 40 \\ 56 \end{pmatrix}$	$\begin{pmatrix} 11.6 \pm 7.5 \\ 8.5 \pm 3.1 \end{pmatrix}$ $\begin{pmatrix} 33 \\ 42 \end{pmatrix}$	$\begin{pmatrix} 63 \\ 74 \end{pmatrix}$	$\begin{pmatrix} 9 \\ 19 \end{pmatrix}$

removed to conduct an overall comparison with the remaining 27 stations with one-time STD (equivalent to 68% confidence level, CL) and to express the deviation of the RMS and correlation coefficient (Cor.) among these stations. The average RMS and average Cor. are listed in Tables 6 and 7, respectively. Table 6 shows that for 63-81% of the stations, the results from the profile approach achieved smaller RMS than those from the pointwise approach. Unlike the pointwise approach, the pro-

Table 7. Comparison of average Cor. and STD over 27 stations given by profile approach (PR) and pointwise approach (PT), and percentage (Per.) of stations where the profile approach results in higher Cor. under different gridding filter radii.

Filter radius	Average Cor. $\pm$ STD $\begin{pmatrix} u_R \\ v_R \end{pmatrix}$		Per. (%) $\begin{pmatrix} u_R \\ v_R \end{pmatrix}$
	PT	PR	
0.72°	$\begin{pmatrix} 0.67 \pm 0.29 \\ 0.41 \pm 0.27 \end{pmatrix}$	$\begin{pmatrix} 0.70 \pm 0.30 \\ 0.48 \pm 0.26 \end{pmatrix}$	$\begin{pmatrix} 70 \\ 74 \end{pmatrix}$
1.00°	$\begin{pmatrix} 0.66 \pm 0.31 \\ 0.41 \pm 0.27 \end{pmatrix}$	$\begin{pmatrix} 0.68 \pm 0.31 \\ 0.47 \pm 0.27 \end{pmatrix}$	$\begin{pmatrix} 63 \\ 78 \end{pmatrix}$
1.13°	$\begin{pmatrix} 0.65 \pm 0.31 \\ 0.40 \pm 0.28 \end{pmatrix}$	$\begin{pmatrix} 0.67 \pm 0.32 \\ 0.46 \pm 0.27 \end{pmatrix}$	$\begin{pmatrix} 63 \\ 74 \end{pmatrix}$

Table 8. Overall cross comparison of our results derived by profile approach and the maps of time-variant surface geostrophic currents from AVISO.

Filter radius	$\begin{pmatrix} u_R \\ v_R \end{pmatrix}$	
	Average RMS $\pm$ STD (cm/s)	Average Cor. $\pm$ STD
0.72°	$\begin{pmatrix} 6.72 \pm 7.55 \\ 6.21 \pm 7.00 \end{pmatrix}$	$\begin{pmatrix} 0.66 \pm 0.23 \\ 0.63 \pm 0.23 \end{pmatrix}$
1.00°	$\begin{pmatrix} 7.02 \pm 7.44 \\ 6.47 \pm 7.03 \end{pmatrix}$	$\begin{pmatrix} 0.59 \pm 0.24 \\ 0.55 \pm 0.24 \end{pmatrix}$
1.13°	$\begin{pmatrix} 7.17 \pm 7.47 \\ 6.60 \pm 7.11 \end{pmatrix}$	$\begin{pmatrix} 0.56 \pm 0.25 \\ 0.51 \pm 0.25 \end{pmatrix}$

file approach yielded a good average RMS of around 8.5-11.6 cm/s and the highest ROI of up to 32%. The resulting average RMS takes about 33-43% and 42-76% of the absolute maximum *in situ* current velocities using the profile and pointwise approaches, respectively. The pointwise approach requires a wider filter radius to achieve higher accuracy.

Through preprocessing, the profile approach mitigates the detrimental effect of omission errors resulting from the discrepancy in the spatial resolution between the along-track SSHs and satellite-only geoid model. As shown in Table 7, the main improvement can be observed in the magnitude of the results but not in the time-variant signal, which shows no significant difference compared with the Cor. of the conventional pointwise approach. Nevertheless, the profile approach still yields a higher Cor. than the pointwise approach at 63-78% of stations. The comparisons clearly indicate that the profile approach outperforms the pointwise approach in determining near-surface time-variant geostrophic current velocities through validation using TAO/TRITON and PIRATA *in situ* current velocities.

To provide a more robust assessment of the performance of profile approach, the maps of time-variant surface geostrophic

currents processed and distributed by AVISO were used for the cross comparison. The global average RMS, Cor. and corresponding STD over 32550 grids, where contain the data over 50% of full time span (over 96 months of data out of 192 months during 1996-2011), were calculated to provide an overall evaluation (Table 8). The comparison shows an overall RMS of 6-7 cm/s with STD of 7 cm/s and Cor. of 0.5-0.6 with STD of 0.2, which are of the same level as the comparison of our results and *in situ* data shows. The discrepancies may come from that AVISO has merged all available satellite observations at given time and assimilated *in situ* hydrographic data and current velocity observations.

2. Validation at Subsurface Layers

The results given by the profile approach with a gridding filter radius of 0.72° were used in the following analysis to retain time-variant signals. The previous section discussed the performance analysis on the profile approach and the validation for the resulting surface geostrophic currents, except for those at the subsurface layers. Therefore, the KESS and Line-W observations were used to validate the resulting subsurface geostrophic currents.

Table 9. Validation of the results at KESS Stations 4 and 5 fixed at 250 m depth. The ratios of the resulting RMS over the absolute maximum in situ current velocities, RMS, and Cor. are also presented.

Station	Ratio (%) $\begin{pmatrix} u_R \\ v_R \end{pmatrix}$	RMS (cm/s) $\begin{pmatrix} u_R \\ v_R \end{pmatrix}$	Cor. $\begin{pmatrix} u_R \\ v_R \end{pmatrix}$
4	$\begin{pmatrix} 34 \\ 29 \end{pmatrix}$	$\begin{pmatrix} 17.88 \\ 20.29 \end{pmatrix}$	$\begin{pmatrix} 0.57 \\ 0.90 \end{pmatrix}$
5	$\begin{pmatrix} 43 \\ 31 \end{pmatrix}$	$\begin{pmatrix} 24.25 \\ 18.41 \end{pmatrix}$	$\begin{pmatrix} 0.78 \\ 0.72 \end{pmatrix}$

Table 10. Validation of the results at seven KESS stations fixed at 1,500 m depth. The average ratios of the results over the absolute maximum in situ current velocities, average RMS, and Cor. are also presented.

Average ratio (%) $\begin{pmatrix} u_R \\ v_R \end{pmatrix}$	Average RMS (cm/s) $\begin{pmatrix} u_R \\ v_R \end{pmatrix}$	Average Cor. $\begin{pmatrix} u_R \\ v_R \end{pmatrix}$
$\begin{pmatrix} 60 \\ 63 \end{pmatrix}$	$\begin{pmatrix} 6.76 \pm 1.64 \\ 7.22 \pm 2.55 \end{pmatrix}$	$\begin{pmatrix} 0.59 \pm 0.26 \\ 0.73 \pm 0.05 \end{pmatrix}$

Table 11. Validation of results at W5 station of Line-W over five depths. The average ratios of the results over the absolute maximum in situ current velocities, average RMS, and Cor. are given.

Average ratio (%) $\begin{pmatrix} u_R \\ v_R \end{pmatrix}$	Average RMS (cm/s) $\begin{pmatrix} u_R \\ v_R \end{pmatrix}$	Average Cor. $\begin{pmatrix} u_R \\ v_R \end{pmatrix}$
$\begin{pmatrix} 45 \\ 67 \end{pmatrix}$	$\begin{pmatrix} 7.47 \pm 0.17 \\ 7.07 \pm 0.11 \end{pmatrix}$	$\begin{pmatrix} 0.47 \pm 0.02 \\ 0.54 \pm 0.02 \end{pmatrix}$

In the observations from KESS Station 4 fixed at 250 m depth, the zonal RMS is 17.88 cm/s, while the meridional RMS is 20.29 cm/s. These values account for 34% and 29% of the absolute maximum *in situ* current velocities with Cor. values of 0.57 and 0.90, respectively. At Station 5, the zonal RMS is 24.25 cm/s, and the meridional RMS is 18.41 cm/s. These values account for 43% and 31% of the absolute maximum *in situ* current velocities with Cor. values of 0.78 and 0.72 (Table 9), respectively. For the seven KESS stations fixed at 1,500 m depth, the average RMS and Cor. were estimated, and the results are presented in Table 10. The average ratios between the RMS and absolute maximum *in situ* current velocity are 60% and 63% in the zonal and meridional directions, respectively. The average RMS are 6.76 and 7.22 cm/s with the average Cor. at 0.59 and 0.73 in the zonal and meridional directions, respectively.

The average RMS and Cor. compared with *in situ* observations at the W5 station of Line-W over five selected depths is

shown in Table 11. The average ratios of RMS over the absolute maximum *in situ* current velocities are 45% and 67% in the zonal and meridional directions, respectively. The average RMS are 7.47 and 7.07 cm/s, with the average Cor. at 0.47 and 0.54 in the zonal and meridional directions, respectively. The current velocities at each depth given by Station W5 only show slight differences.

The validation of the subsurface geostrophic currents indicates an absolute RMS of around 20 cm/s at a depth of 250 m for the KESS Station 4 and 5 observations. The average RMS of the *in situ* observations at deeper layers (seven KESS stations fixed at 1,500 m depth and Station W5 of Line-W under 1,000 m depth) is around 7 cm/s. The Cor. ranges from around 0.5 and to 0.9, which is indicative of the good temporal agreement with the *in situ* observations. Fig. 5 shows the time series of the resulting and *in situ* subsurface currents at stations W5 of Line-W with the longest temporal span of four years among all the in situ observations we used. General conformity
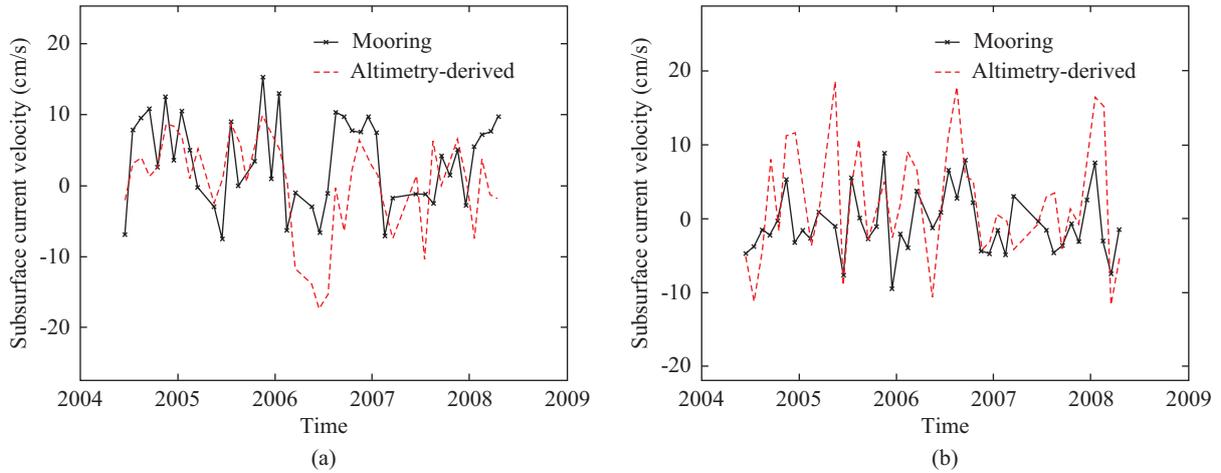
Fig. 5. Time series of (a) zonal and (b) meridional current velocities at Station W5 of Line-W fixed at 1,500 m depth.
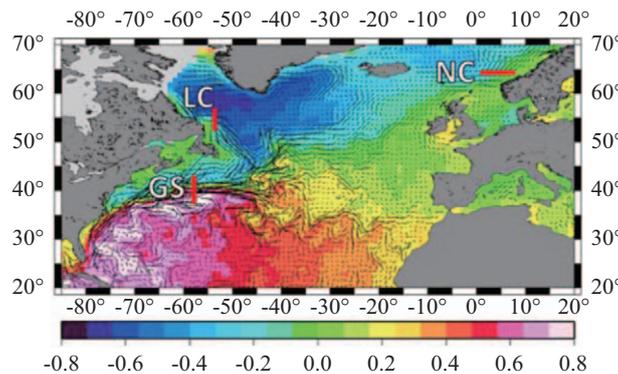

Fig. 6. Multi-satellite determined absolute dynamic topography (color) and surface geostrophic currents (black vector) in January 1996. Sections (thick red lines) selected through the pathway of GS (38.5°-41.5°N, 300.5°E), NC (64.5°N, 0.5°-6.5°E), and LC (53.5°-56.5°N, 305.5°E).

in temporal pattern can be seen. The interannual variations are related to changes of hydrographic properties (Peña-Molino et al., 2012). Since not only the comparatively placid RDT but also ADT, retaining the significant surface gradients, are involved in the determination of subsurface geostrophic currents, the results were inextricably affected by the signal from the rougher sea surface which leads to stronger amplitude in temporal variation compared with that in the in situ observations directly collected at the deeper ocean. On the other hand, our understanding toward the deep oceanic properties are still relatively limited due to difficulties in deployment of instruments, hence, the RDT may contain larger errors propagated from the hydrographic data at deeper layer.

1. Relations of Geostrophic Currents and North Atlantic Oscillation

In the North Atlantic Ocean, the GS, the upper limb of the AMOC, transports warm Atlantic waters from the low-latitude regions to the high-latitude regions, where the Norwegian Current (NC) further carries the heat to the Arctic region. The Labrador Current (LC) brings cold polar waters originating from the Arctic back to the mid-latitude. Each branch is functional and plays a critical role. Here, sections through the current pathways of (1) GS, (2) NC, and (3) LC were selected to study the correlation of ocean current changes with the NAO climate index (Fig. 6).

The annual mean GS current speeds show a maximum correlation with the NAO of 0.5-0.7, which is significant at the 95-99% confidence level (CL), with a two-year lag in the upper 600 m depth (Fig. 7(a)). The significant correlation is thought to be linked to the latitudinal shift of the GS pathway (Taylor and Stephens, 1998), which estimated a maximum correlation of 0.55 with a two-year lag. Gangopadhyay et al. (1992) suggested that the time lag is related to the time for the baroclinic Rossby wave to traverse the ocean.

After removing the trend, semi-annual, and annual cycle, a 13-month moving average filter was applied to the time series of the monthly current speeds and climate index to reduce residual intra-annual noise, for correlation studies. The estimated maximum correlation between the monthly NC current speeds and the NAO is 0.6-0.4, which decreases with depth, with a NC time lag of two months, which is significant at the
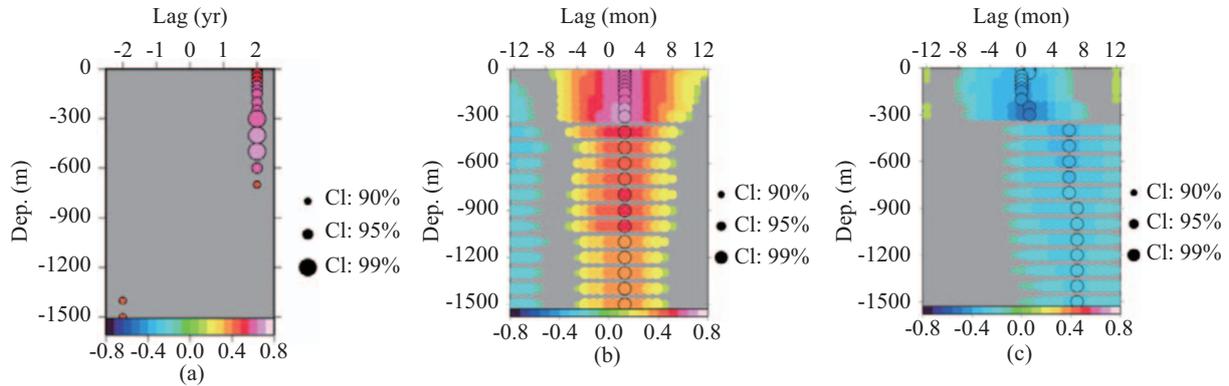
Fig. 7. Depth-lag correlation map of surface and subsurface geostrophic current speeds between (a) annual Gulf Stream (GS), monthly (b) Norwegian Current (NC), (c) Labrador Current (LC), and the North Atlantic Oscillation (NAO) index.

99% CL (Fig. 7(b)). Dickson et al. (1996) indicated that changes in the intensity of the northward-flowing NC have been linked to variability in the NAO pattern. The experiments using the atmospheric conditions of 1979 (negative phase of the NAO) and 1990-1994 (positive phase of the NAO) show the deeper penetration of warmer, fresher, and stronger Atlantic waters carried by the NC in the positive phase of the NAO and be opposite in the negative phase of NAO (Dickson, 1999). According to Venegas and Mysak (2000), the transport of heat by the NC into the Arctic region is stronger during the periods with a positive NAO. Atlantic waters do not reach so far north when the NAO is negative. The highly positive correlation between the NC and the NAO reflects these facts.

The correlation between the monthly LC current speeds and the NAO was also estimated. The maximum correlation between the monthly LC current speed and the NAO is -0.2 to -0.5, which is significant at the 99% CL, with an LC time lag of 0-7 months from the surface to the deeper layer (Fig. 7(c)). According to Rossby and Benway (2000), regional thermohaline processes between the Labrador Sea and the Labrador Shelf can significantly weaken the density-driven LC in the summer following a positive NAO winter; by contrast, a negative NAO winter leads to weak westerlies over the Labrador Sea strengthening the LC, in which case a negative correlation exists between the LC and NAO, which conforms to our estimation. Given the strong (weak) LC results in the southward (northward) shift of the GS pathway (Rossby, 1999), the negative correlation also complies with the positive correlation between the GS and NAO. The current speeds through the sections of the AMOC are correlated with the NAO at a statistically significant level that complies with oceanographic facts.

V. CONCLUSIONS

Previous studies all used the GOCE geoid model as MDT datum to conduct the analysis of mean surface geostrophic currents. Here, our study combined multiple radar altimetry 1 Hz along-track SSHs, the GOCE satellite-only geoid model, and *in situ* hydrographic profiles to extend the prior determi-

nation of surface geostrophic currents to include the subsurface layers globally, with enhanced spatial resolutions combining two distinct repeat orbits generated SSHs, over a decade and a half (1996-2011). The estimated velocities were verified using *in situ* current meter observations from the numerous near-surface moored stations of TAO/TRITON and PIRATA across the tropical Pacific and Atlantic Ocean. Comparisons were aimed at analyzing the performance of the different processing strategies for dealing with the detrimental effect of omission errors resulting from the use of the truncated satellite-only geoid model as datum of SSHs. By using a profile approach, the determination of geostrophic current velocities with higher accuracy than the conventional pointwise approach can be achieved with significant improvement near the ocean-land boundary and with reduced effects of omission errors. The resulting subsurface geostrophic currents have been validated by *in situ* observations from stations deployed by the KESS and Line-W projects. The comprehensive performance estimation shows good agreement.

With estimated surface and subsurface geostrophic current velocities at different depth layers and spanning over 15 years, we study their correlations with NAO index, with selected sections across branches of the Atlantic Meridional Overturning Circulation (AMOC), including the Gulf Stream, the Norwegian Current and the Labrador Current. Each of these currents has a significant positive or negative correlations with the NAO with statistically significant confidence level (CL) at 95-99%. Our results in the North Atlantic are in general agreements with results of other studies, that the response of ocean current systems are correlated with NAO index in the form of pathway shift and variation in current velocities.

REFERENCES

Bingham, R. J., K. Haines and C. W. Hughes (2008). Calculating the ocean's mean dynamic topography from a mean sea surface and a geoid. Journal of Atmospheric and Oceanic Technology 25, 1,808-1,822.

Bosch, W. and R. Savcenko (2010). On estimating the dynamic ocean topography - a profile approach, In: Gravity, Geoid and Earth Observation, edited by Mertikas, S. P., International Association of Geodesy Symposia 135, 263-269.

Bosch, W., R. Savcenko, D. Dettmering and C. Schwatke (2012). A two-decade time series of eddy-resolving dynamic ocean topography (iDOT), in Proceedings of the Symposium on 20 Years of Progress in Radar Altimetry, Venice, Italy, ESA SP-710[CD-ROM].

Bourles, B., R. Lumpkin, M. J. McPhaden, F. Hernandez, P. Nobre, E. Campos, L. Yu, S. Planton, A. Busalacchi, A. D. Moura, J. Servain and J. Trotte (2008). The PIRATA program: History, accomplishments, and future directions. Bulletin of the American Meteorological Society 89, 1,111-1,125.

Bright, R. J., L. Xie and L. J. Pietrafesa (2002). Evidence of the Gulf Stream's influence on tropical cyclone intensity. Geophysical Research Letters 29, 16, 48-1-48-4.

Bruinsma, S. L., C. Förste, O. Abrikosov, J.-C. Marty, M.-H. Rio, S. Mulet and S. Bonvalot (2013). The new ESA satellite-only gravity field model via the direct approach. Geophysical Research Letters 40, 14, 3,607-3,612.

Cabanes, C., A. Grouazel, K.von Schuckmann, M. Hamon, V. Turpin, C. Coatanoan, F. Paris, S. Guinehut, C. Boone, N. Ferry, C. de Boyer Montégut, T. Carval, G. Reverdin, S. Pouliquen and P.-Y. Le Traon (2013). The CORA dataset: validation and diagnostics of *in-situ* ocean temperature and salinity measurements. Ocean Science 9, 1, 1-18.

Cadden, D. D. H., B. Subrahmanyam, D. P. Chambers and V. S. N. Murty (2009). Surface and subsurface geostrophic current variability in the Indian Ocean from altimetry. Marine Geodesy 32, 19-29.

Chambers, D. P., B. D. Tapley and R. H. Stewart (1997). Long-period ocean heat storage rates basin-scale heat fluxes from TOPEX. Journal of Geophysical Research 102, 10,525-10,533.

Dickson, B. (1999). All change in the Arctic, Nature, 397, 389-391.

Dickson, R., J. Lazier, J. Meincke, P. Rhines and J. Swift (1996). Long-term coordinated changes in the convective activity of the North Atlantic. Progress in Oceanography 38, 241-295.

ESA (1999). Gravity Field and Steady-State Ocean Circulation Mission, Reports for Mission Selection 'The Four Candidate Earth Explorer Core Missions', ESA SP-1233(1), Noordwijk, Netherland.

Ezer, T., L. P. Atkinson, W. B. Corlett and J. L. Blanco (2013). Gulf Stream's induced sea level rise and variability along the U.S. mid-Atlantic coast. Journal of Geophysical Research: Oceans 118, 685-697.

Feng, G., S. Jin, and J. M. Sánchez-Reales (2013). Antarctic circumpolar current from satellite gravimetric models ITG-GRACE2010, GOCE-TIM3 and satellite altimetry. Journal of Geodynamics 72, 72-80.

Gangopadhyay, A., P. Cornillon and R. Watts (1992). A test of the Parsons-Veronis hypothesis on the separation of the Gulf Stream. Journal of Physical Oceanography 22, 1,286-1,301.

Hansen, D. V. and P.-M. Poulain (1996). Quality control and interpolation of WOCE-TOGA drifter data. Journal of Atmospheric and Oceanic Technology 13(4), 900-909.

Heiskanen, W. A. and H. Moritz (1967). Physical Geodesy, W. H. Freeman and Company, San Francisco.

Hurrell, J. W. (1995). Decadal trends in the North Atlantic Oscillation: Regional temperatures and precipitation. Science 269, 676-679.

Ishii, M. and M. Kimoto (2009). Reevaluation of historical ocean heat content variations with time-varying XBT and MBT depth bias corrections. Journal of Oceanography 65, 287-299.

Janjić, T., J. Schröter, R. Savcenko, W. Bosch, A. Albertella, R. Rummel and O. Klatt (2012). Impact of combining GRACE and GOCE gravity data on ocean circulation estimates. Ocean Science 8, 65-79.

Jayne, S. R., N. G. Hogg, S. N. Waterman, L. Rainville, K. A. Donohue, D. R. Watts, J.-H. Park, J. L. McClean, M. E. Maltrud, B. Qiu, S. Chen and P. Hacker (2009). The Kuroshio Extension and its recirculation gyres. Deep-Sea Research Part I, 56, 2,088-2,099.

Jekeli, C. (1981). Alternative methods to smooth the earth's gravity field, Report 327, Department of Geodetic Science and Surveying, Ohio State University, Columbus, Ohio, U.S.A.

Lagerloef, G. S. E., G. T. Mitchum, R. B. Lukas and P. P. Niiler (1999). Tropical Pacific near-surface currents estimated from altimeter, wind, and drifter data. Journal of Geophysical Research 104, 23,313-23,326.

Lukas, R. and E. Firing (1984). The geostrophic balance of the Pacific Equatorial Undercurrent. Deep-Sea Research Part A, 31, 61-66.

Mayer-Gürr, T. (2007). ITG-Grace03s: The latest GRACE gravity field solution computed in Bonn. Joint International GSTM and SPP Symposium, Postdam, Germany, 15-17 October.

McPhaden, M. J., A. J. Busalacchi, R. Cheney, J.-R. Donguy, K. S. Gage, D. Halpern, M. Ji, P. Julian, G. Meyers, G. T. Mitchum, P. P. Niiler, J. Picaut, R. W. Reynolds, N. Smith and K. Takeuchi (1998). The tropical ocean-global atmosphere observing system: A decade of progress. Journal of Geophysical Research 103, 14,169-14,240.

Millero, F. J. and A. Poisson (1981). International one-atmosphere equation of state of sea-water. Deep-Sea Research 28, 625-629.

Ohashi, Kyoko, G. Han, N. Chen and J. Helbig (2013). Northwest Atlantic surface circulation from multi-satellite observations. Atmosphere-Ocean 51, 35-49.

Pail, R., S. Bruinsma, F. Migliaccio, C. Förste, H. Goiginger, W.-D. Schuh, E. Höck, M. Reguzzoni, J. M. Brockmann, O. Abrikosov, M. Veicherts, T. Fecher, R. Mayrhofer, I. Krasbutter, F. Sansó and C. C. Tscherning (2011). First GOCE gravity field models derived by three different approaches. Journal of Geodesy 85, 819-843.

Pavlis, N. K., S. A. Holmes, S. C. Kenyon and J. K. Factor (2012). The development and evaluation of the Earth Gravitational Model 2008 (EGM2008). Journal of Geophysical Research: Solid Earth (1978-2012) 117, B04406, DOI: 10.1029/2011JB008916.

Peña-Molino, B., T. M. Joyce and J. M. Toole (2012). Variability in the Deep Western Boundary Current: Local versus remote forcing. Journal of Geophysical Research 117, C12022, DOI: 10.1029/2012JC008369.

Picaut, J., S. P. Hayes and M. J. McPhaden (1989). Use of the geostrophic approximation to estimate time-varying zonal currents at the equator. Journal of Geophysical Research 94, 3,228-3,236.

Rio, M.-H., S. Mulet, E. Greiner, N. Picot, A. Pascual (2013). New global mean dynamic topography from a GOCE geoid model, altimeter measurements and oceanographic *in-situ* data, Ocean Surface Topography Science Team Meeting and 7th Coastal Altimetry Workshop, Boulder, Colorado, U.S.A., 8-11, October.

Rossby, T. (1999). On gyre interactions, Deep Sea Research Part II, 46, 139-164.

Rossby, T. and R. L. Benway (2000). Slow variations in mean path of the Gulf

Stream east of Cape Hatteras, Geophysical Research Letters 27, 117-120.

Sánchez-Reales, J. M., M. I. Vigo, S. Jin and B. F. Chao (2012). Global surface geostrophic ocean currents derived from satellite altimetry and GOCE geoid. Marine Geodesy 35, 175-189.

Scharroo, R., E. W. Leuliette, J. L. Lillibridge, D. Byrne, M. C. Naeije and G. T. Mitchum (2013). RADS: Consistent multi-mission products, in Proceedings of the Symposium on 20 Years of Progress in Radar Altimetry, Venice, Italy, ESA SP-710[CD-ROM].

Taylor, A. H. and J. A. Stephens (1998). The North Atlantic Oscillation and the latitude of the Gulf Stream. Tellus A 50, 134-142.

Venegas, S. A. and L. A. Mysak (2000). Is there a dominant timescale of natural climate variability in the Artic? Journal of Climate 13, 3,412-3,434.

Waterman, S. N., N. G. Hogg and S. R. Jayne (2011). Eddy-mean interaction in the Kuroshio Extension region. Journal of Physical Oceanography 41, 1,182-1,208.

Weber, J. E. (1983). Steady wind- and wave-induced currents in the open ocean. Journal of Physical Oceanography 13, 524-530.

Wessel, P., and W. H. F. Smith (1991). Free software helps map and display data. Eos Transaction. AGU 72, 441-446.

Wunsch, C. and E. M. Gaposchkin (1980). On using satellite altimetry to determine the general circulation of the oceans with application to geoid improvement. Reviews of Geophysics 18, 725-745.

Zenner, L (2006). Zeitliche schwerefeldvariationen aus GRACE und hydrologiemodellen, Diplomarbeit on TU München, Institut für Astronomische und Physikalische Geodäsie.

Zhang, H. M., J. J. Bates and R. W. Reynolds (2006a). Assessment of composite global sampling: Sea surface wind speed. Geophysical Research Letter 33, L17714, DOI: 10.1029/2006GL027086.

Zhang, H. M., R. W. Reynolds and J. J. Bates (2006b). Blended and gridded high resolution global sea surface wind speed and climatology from multiple satellites: 1987-present, American Meteorological Society 2006 Annual Meeting, Atlanta, GA. Paper 100004.